

# Northumbria Research Link

Citation: Roncallo, Scilla, Painter, Jonathan, Healy, Matthew, Ritchie, Simon, Finnis, Mark, Rogers, Keith, Scragg, Jonathan, Dale, Phillip and Zoppi, Guillaume (2011) Effects of different needles and substrates on CuInS<sub>2</sub> deposited by electrostatic spray deposition. Thin Solid Films, 519 (11). pp. 3544-3551. ISSN 00406090

Published by: Elsevier

URL: <http://dx.doi.org/10.1016/j.tsf.2011.01.248>  
<<http://dx.doi.org/10.1016/j.tsf.2011.01.248>>

This version was downloaded from Northumbria Research Link:  
<http://nrl.northumbria.ac.uk/id/eprint/349/>

Northumbria University has developed Northumbria Research Link (NRL) to enable users to access the University's research output. Copyright © and moral rights for items on NRL are retained by the individual author(s) and/or other copyright owners. Single copies of full items can be reproduced, displayed or performed, and given to third parties in any format or medium for personal research or study, educational, or not-for-profit purposes without prior permission or charge, provided the authors, title and full bibliographic details are given, as well as a hyperlink and/or URL to the original metadata page. The content must not be changed in any way. Full items must not be sold commercially in any format or medium without formal permission of the copyright holder. The full policy is available online: <http://nrl.northumbria.ac.uk/policies.html>

This document may differ from the final, published version of the research and has been made available online in accordance with publisher policies. To read and/or cite from the published version of the research, please visit the publisher's website (a subscription may be required.)

## Accepted Manuscript

Effects of different needles and substrates on  $\text{CuInS}_2$  deposited by Electrostatic Spray Deposition

S. Roncallo, J.D. Painter, M.J.F. Healy, S.A. Ritchie, M.V. Finnis, K.D. Rogers, J.J. Scragg, P.J. Dale, G. Zoppi

PII: S0040-6090(11)00311-7  
DOI: doi: [10.1016/j.tsf.2011.01.248](https://doi.org/10.1016/j.tsf.2011.01.248)  
Reference: TSF 28780

To appear in: *Thin Solid Films*

Received date: 11 February 2010  
Revised date: 12 January 2011  
Accepted date: 12 January 2011



Please cite this article as: S. Roncallo, J.D. Painter, M.J.F. Healy, S.A. Ritchie, M.V. Finnis, K.D. Rogers, J.J. Scragg, P.J. Dale, G. Zoppi, Effects of different needles and substrates on  $\text{CuInS}_2$  deposited by Electrostatic Spray Deposition, *Thin Solid Films* (2011), doi: [10.1016/j.tsf.2011.01.248](https://doi.org/10.1016/j.tsf.2011.01.248)

This is a PDF file of an unedited manuscript that has been accepted for publication. As a service to our customers we are providing this early version of the manuscript. The manuscript will undergo copyediting, typesetting, and review of the resulting proof before it is published in its final form. Please note that during the production process errors may be discovered which could affect the content, and all legal disclaimers that apply to the journal pertain.

# Effects of different needles and substrates on $\text{CuInS}_2$ deposited by Electrostatic Spray Deposition

S. Roncallo\*, J.D. Painter<sup>\*a</sup>, M.J.F. Healy\*, S. A. Ritchie<sup>+</sup>, M.V. Finnis<sup>+</sup>, K. D.

Rogers<sup>-</sup>, J.J. Scragg<sup>b</sup>, P.J. Dale<sup>c</sup>, G. Zoppi<sup>d</sup>

*\* Centre for Materials Science and Engineering, Cranfield University,  
Shrivenham, Swindon, SN6 8LA, UK*

*+ Department of Engineering Systems and Management, Cranfield University,  
Shrivenham, Swindon SN6 8LA, UK*

*- Cranfield Health, Cranfield University, Cranfield, Bedfordshire, MK43 0AL, UK*

*<sup>b</sup> University of Bath, Claverton Down, Bath, BA2 7AY, UK*

*<sup>c</sup> Laboratoire Photovoltaïque, University of Luxembourg, 41 Rue du Brill, L-4422,  
Belvaux, Luxembourg*

*<sup>d</sup> Northumbria Photovoltaics Applications Centre, Northumbria  
University, Newcastle Upon Tyne NE1 8ST, UK*

<sup>a</sup> Corresponding Author

Email address: j.d.painter@cranfield.ac.uk

## Abstract

Copper indium disulphide ( $\text{CuInS}_2$ ) thin films were deposited using the electrostatic spray deposition method. The effects of applied voltage and solution flow rate on the aerosol cone shape, film composition, surface morphology and

current conversion were investigated. The effect of aluminium substrates and transparent fluorine doped tin oxide ( $\text{SnO}_2\text{:F}$ ) coated glass substrates on the properties of as-deposited  $\text{CuInS}_2$  films were analysed. An oxidation process occurs during the deposition onto the metallic substrates which forms an insulating layer between the photoactive film and substrate. The effects of two different spray needles on the properties of the as-deposited films were also studied. The results reveal that the use of a stainless steel needle results in contamination of the film due to the transfer of metal impurities through the spray whilst this is not seen for the glass needle. The films were characterised using a number of different analytical techniques such as X-ray diffraction, scanning electron microscopy, Rutherford back-scattering and secondary ion mass spectroscopy and opto-electronic measurements.

### **Keywords**

$\text{CuInS}_2$ , electrostatic spray deposition (ESD), coating uniformity, solar cells, deposition conditions, needles, substrates

## **1 Introduction**

Photovoltaic devices are one of a number of environmentally friendly forms of generating electricity that are undergoing significant research and development. The main barrier to the widespread use of this form of energy over the last few decades has been the high unit energy cost of production. A reduction in turn-key photovoltaic system prices and further technological developments are

necessary to allow the cell manufacturers to strengthen their position in the global market. The increasing demand for 'green' materials in solar cell production has raised the profile and hence the research interest in  $\text{CuInS}_2$ -based cells due to their inherently non-toxic composition.  $\text{CuInS}_2$  (CIS) is a very attractive material for device fabrication because it has a band gap of about 1.5 eV which is close to the theoretical optimum value for single junction solar cells; CIS is a direct band gap semiconductor thus 1  $\mu\text{m}$  thick films are able to absorb all the incident photons (with an energy greater than the band gap) of the solar spectrum; it also has non-degradable properties compared with other solar cell materials [1, 2].  $\text{CuInS}_2$  is a ternary chalcogenide semiconductor which can behave as an n-type or p-type material by varying the molar ratios of the compositional elements [3, 4]. Highest theoretical efficiency (25%) [5] is attributed to  $\text{CuInS}_2$ , although the experimental record (nearly 20%) has been achieved in single junction CIGS  $[\text{Cu}(\text{In,Ga})-(\text{Se,S})_2]$  solar cell absorbers [6]. A number of methods have been used to deposit chalcopyrite CIS thin films such as molecular vacuum methods [7], radio frequency sputtering [8], single source evaporation [9], electrochemical deposition [10,11], spray pyrolysis [12]. Electrostatic spray deposition (ESD) is a simple, non-vacuum method which uses an applied voltage between a spray needle and a substrate to atomise a chemical solution. The droplets of solution undergo a complex decomposition-reaction process which yields the deposition of dense films with good adhesion to the substrate. This method allows good control of stoichiometry and film thickness resulting in high quality CIS samples which do not require a post

deposition anneal. In this paper, the deposition of  $\text{CuInS}_2$  films using different types of spray needle (stainless steel and glass) is reported. The effect of different deposition conditions on films grown on various substrates (aluminium and  $\text{SnO}_2\text{:F}$  coated glass) are also considered. In both cases, the structural, compositional and opto-electronic properties of the as-deposited films were analysed using various characterisation techniques.

## 2 Experimental Details

$\text{CuCl}_2 \cdot 2\text{H}_2\text{O}$  (99.99%, Sigma Aldrich),  $\text{InCl}_3$  (99.99%, Alfa Aesar) and thiourea (99%, Alfa Aesar) were dissolved in deionised water ( $18 \text{ MWcm}^{-1}$  at  $25^\circ\text{C}$ ). During this experiment, the solution concentration was maintained at 0.21 M while the  $[\text{S}]/[\text{Cu}]$  and  $[\text{Cu}]/[\text{In}]$  molar ratios were fixed at 5 and 1 respectively [13]. HCl was added to facilitate the dissolution of the three salts. Two different experiments were carried out during the study in order to analyse the effect of changing the substrate and needle materials independently.

Full details of the deposition setup have been given elsewhere [14,15].

During the initial experiment, the starting solutions were sprayed onto two different substrates: aluminium (Al) and  $\text{SnO}_2\text{:F}$  coated glass using the glass needle. The glass needle (produced in house) had a platinum wire embedded through the wall in order to make an electric contact with the high voltage source and atomise the solution as it passed over the wire. The substrates had dimensions of 1.8 mm x 30 mm x 10 mm in thickness, length and depth, respectively. Deposition temperature, needle-substrate distance and solution

concentration were fixed at 450°C, 50 mm and 30 mM respectively. The precursor solution was atomised using a positive applied voltage which was varied between 14 kV and 18 kV. The flow rate was varied between 25  $\mu\text{l}/\text{min}$  and 100  $\mu\text{l}/\text{min}$  and the deposition time was set to spray 18 ml in total. This resulted in spray times between 3 and 12 hours. The effects of these two depositions variables on the properties of CIS thin films have been examined. All the aluminium samples were polished using sandpaper (up to 2500 grit) and a 6 micron diamond suspension reduced to 1 micron for final polishing. The glass substrate used for deposition was commercially available Nippon  $\text{SnO}_2\text{:F}$  transparent coated glass (FTO).

During the second experiment, CIS films were deposited using both stainless steel and glass needles. The stainless steel hypodermic needle had an external diameter of 0.5 mm and a 0.1 mm wall thickness. The tip of the needle was flattened prior to use to remove the sharp tip, which otherwise caused arcing between the needle and substrate. The external diameter of the glass needle at the tip was 0.6 mm with a wall thickness of approximately 0.1 mm. During this experiment all the samples were deposited on  $\text{SnO}_2\text{:F}$  coated glass substrates.

The structural, compositional and opto-electronic properties of the as-deposited films were analysed. The techniques used were X-ray diffraction (XRD), scanning electron microscopy (SEM), Rutherford Backscattering Spectrometry (RBS), secondary ion mass spectrometry (SIMS) and photocurrent conversion. In addition laser particle visualisation (PIV) was used to monitor the properties of the spray cone.

XRD was performed using a Philips PW1820 diffractometer with Cu-K $\alpha$  radiation ( $\lambda = 1.5405 \text{ \AA}$ ). Standard  $\theta - 2\theta$  diffraction data was collected over the range  $10^\circ < 2\theta < 80^\circ$  with a scan step size of  $0.02^\circ$  and 5 s count time. Additionally glancing angle XRD was undertaken on selected samples with  $\theta$  fixed at  $5^\circ$  and  $2\theta$  scanned between  $10$  and  $80^\circ$  with a step size of  $0.02^\circ$  and count time of 5 s. Identification of the phases in each diffraction pattern was performed with reference to the powder diffraction file (PDF) database from the International Centre for Diffraction Data. SEM analysis was conducted using either a JEOL JSM840A or LEO 435VP with an accelerating voltage of 15 kV.

The elemental composition and thickness of the thin films were analysed using RBS which was carried out using a 1.9 MeV  $^3\text{He}^+$  ion beam generated from a Van de Graaff generator in conjunction with a multi-channel analyzer with a system resolution of 25 keV. The detector was positioned at a back scattering angle of  $170^\circ$  with a collection solid angle of 5 m sr. RBS allows the atomic areal density of each element in the film to be determined independently of chemical bonding and, thus, the film thickness if the density is known. RBS measurements were only conducted on films deposited onto Al substrates. No measurements were made on films deposited onto FTO / glass as the underlying complexity of the substrate composition would introduce overlapping 'peaks' and thus large errors when determining CIS element ratios.

Depth profiling of lateral uniformity of the layers were investigated in detail using a bench-top Millbrook MiniSIMS system with a  $\text{Ga}^+$  primary ion energy of 6 keV,



a crater area of  $100\ \mu\text{m} \times 100\ \mu\text{m}$  and a gating of 10%. The measurement yields a qualitative analysis and is not calibrated to give absolute concentrations.

Photoelectrochemical measurements of the  $\text{CuInS}_2$  thin films were performed in aqueous 0.2 M europium nitrate (99.9%, Strem).

The pH was adjusted to 2 by adding  $\text{HNO}_3$ . Measurements were carried out in a three electrode configuration using a glass cell with a  $\text{Ag|AgCl}$  reference electrode, and a platinum foil as a counter electrode. Photovoltammograms were recorded using an Autolab 20 potentiostat under pulsed white light illumination provided by a light emitting diode (LED). Photocurrent spectra were recorded with a standard photoelectrochemical setup: lamp, monochromator, and chopper (Bentham); purpose-built potentiostat, function generator (Hi-Tek); lock-in amplifier (Stanford Research Systems). Spectra were recorded using chopped illumination with a frequency of 13 Hz or higher and normalized against a calibrated silicon photodiode.

The laser particle visualisation was based on particle image velocimetry (PIV) method for measuring flow structures and velocities in particle laden flows. The particles within the aerosol are illuminated periodically by a pulsed laser light source which has its incident beam focused into a planar light sheet (Figure 1). The particles illuminated by the light sheet are imaged normal to the plane of the light sheet using a high frame rate Charge-Coupled Device (CCD) camera and can be analysed off-line to extract particle size and flow structure information.

The laser used during this experiment was a New Wave Gemini Nd:YAG pulsed laser (15 Hz double pulse rate) in conjunction with a Kodak ES1.0 CCD camera. The energy of the light source was 120 mJ per pulse at  $\lambda = 532$  nm.

### 3 Results

#### 3.1 Effects of different substrates

##### 3.1.1 Glass

The FTO coated substrates were chosen due to their higher stability and hence higher resistance to oxidation compared to  $\text{SnO}_2:\text{In}$  coated glass [16]. The deposition conditions of CIS films on FTO glass substrates are summarized in Table 1.

The standard  $\theta - 2\theta$  XRD patterns of samples deposited on FTO at different voltages and flow rates are typical of CIS with no other extraneous phases such as  $\text{Cu}_x\text{S}$  or  $\text{In}_x\text{S}_y$ . An example of an XRD diffractogram for a CIS sample is shown in Figure 2. All the peaks have been assigned to the CIS chalcopyrite structure (or to the FTO substrate).

The as-deposited films do not show a preferred orientation because the intensity ratios of the peaks match the corresponding theoretical intensity ratios, also the area and the FWHM of the (112) CIS peak are similar for all the samples deposited on glass suggesting an independency of grain size from the deposition condition. Figure 3 shows an SEM image of the cross-section of the CIS film on FTO glass (sample G3) deposited using an applied voltage of 18kV. The CIS

absorber layer in this sample has a thickness of approximately 1.8  $\mu\text{m}$ . The image depicts a dense film with good adhesion to the substrate. All samples deposited at 18 kV were similarly adherent.

SEM analysis of the surfaces of films deposited at lower voltages (14 kV and 16 kV) show cracks and defects. The sample G7 (14 kV) is shown in Figure 4 as an example. The applied voltage and flow rate controls the size of the incoming droplets incident on the substrate [13-17]. At low voltage and high flow rate, “big droplets” arrive on the hot substrate but the solvent doesn’t evaporate immediately, leaving a thin liquid layer on the substrate. This phenomenon induces a mechanical stress in the film when the evaporation process is completed. When the solvent evaporates, a change in volume will occur. Since the layer is not able to shrink freely due to the adhesion on the substrates, cracks appear on the films. Figure 4 shows the details of the cracks and defects in the film and the regions where poor adhesion of the film has resulted in the film breaking away from the layers beneath. The indented regions on the surface of the film are thought to be caused by large droplets reaching the substrate. The evaporation of the solvent in the droplets leaves the resulting ‘pin-holed’ film structure.

These results are in good agreement with previous results published by other groups [18-20].

The external quantum efficiency (EQE) of the films was measured as a function of wavelength to see which deposition conditions produced the most photoactive

films suitable for use in photovoltaic devices. A europium electrolyte was used to collect photo excited charge carriers from the films [9]. Figure 5 shows the data for the most photoactive film, G3, which has a maximum EQE of 35 % at 425 nm, which then reduces quickly at longer wavelengths. The EQE dropped to 28 % at 425 nm for film G2, which was grown at twice the speed as film G3. Films deposited at lower voltages G4-G9, despite the pinholes and cracks, gave EQE values of around 25 %. The films were then etched in 5 wt % aqueous KCN and re-tested to see if this improved their photoresponse. KCN is a well know etching solution for  $\text{CuInS}_2$  layers which are grown under copper excess. The KCN etch removes undesired  $\text{Cu}_x\text{S}_y$  preferentially [20-22]. No improvement in the EQE was observed, suggesting that the films contained no  $\text{Cu}_x\text{S}_y$  at the surface, in agreement with the XRD ( $\theta$  -  $2\theta$  and glancing angle) measurements.

Maximum achievable EQE values are only 75 % for high quality  $\text{Cu(In,Ga)Se}_2$  absorber layers. The loss of 25 % is due to optical reflection from the cell configuration. In the films in this study, the lower maximum values of EQE at short wavelengths indicate that there is recombination near the surface of the semiconductor. Also, the reduction of EQE at longer wavelengths indicates either a small space charge region or poor collection of carriers generated outside the space charge region, possibly due to residual chlorine left over from the deposition process

The band gap ( $E_g$ ) of the films was calculated from the EQE spectra using the Gartner equation [23]. An example of the fit is shown in the inset of Figure 5 for

sample G3. For samples G1 to G3 an  $E_g$  value of  $1.45 \pm 0.02$  eV was found, in agreement with other groups.

### 3.1.2 Aluminium substrate

The deposition conditions considered for film spraying onto aluminium substrates are summarised in Table 2.

The XRD patterns for the 9 samples sprayed onto an aluminium substrate display the three main CIS peaks ((112), (220) and (312)) although the intensity is weak (XRD of sample A3 is shown in Figure 6 and Figure 7 as an example). The preferred orientation can be calculated from the intensity values. The intensity ratios of the peaks (220) and (112) (called  $I_2/I_1$ ), (312) and (112) (called  $I_3/I_1$ ), (312) and (220) (called  $I_3/I_2$ ) were calculated for the samples and compared with the theoretical values. It is observed that the ratios  $I_2/I_1$  and  $I_3/I_1$  have values lower than random powder, while the ratios  $I_3/I_2$  are similar for all the samples. The higher intensity of the  $I_1$  peaks suggests a preferred orientation along the (112) plane. Some additional peaks also appear in the diffractograms of CIS films sprayed onto aluminium substrates (Figure 7). The number of these peaks has been observed to be inversely proportional to the applied voltage but appears to be independent of solution flow rate. The intensity of the peaks is small and thus they are difficult to positively identify. They could be due to an aluminium oxide layer formed during the deposition process. The acidic solution which for low voltages may not completely evaporate prior to arriving at the

substrate could corrode the aluminium producing an oxide layer between the substrate and CIS film.

The thickness of the samples was determined by RBS analysis. The RBS measurements have been performed using a detector solid angle of 5 msr and 170 ° back scattering angle. RBS spectra of the sample Al3 is shown in Figure 8. The spectra were modelled using SIMNRA software [24] to generate the simulation. The spectra show the combined contributions of the CIS layer and the aluminium substrate but a tail on the back edge of the Cu and S peaks was observed in all the samples and it is thought to be due to the large roughness of the CIS layer which is characteristic of the deposition method.

The RBS spectra were fitted assuming the presence of a single homogeneous layer of CIS on the aluminium substrate. The stoichiometry of the samples deposited on aluminium appears to have a large variation (Table 3) with no clear trend. It is unclear whether the non-stoichiometric films contain secondary phases. Neither standard  $\theta - 2\theta$  XRD nor glancing angle XRD detected any extraneous phases but small amounts of secondary phases (ie below the detection levels) could feasibly be present.

The nominal target growth thickness of the as-deposited films was 500 nm (based on the density of CIS = 4.748 g/cm<sup>3</sup>), and all but two films (sample Al7 and Al8) grown under a range of deposition conditions lay within +/- 25 % of this

thickness. This could be due to a reduction in the diameter of the spray cone resulting in a higher solution volume per unit area incident on the substrate.

The photo-response of the samples have been studied using three probe configuration photo-voltammetry, europium nitrate solution and a white LED as the light source. None of the samples deposited on aluminium showed any photocurrent response. This is probably because a thin aluminium oxide layer forms between the substrate and CIS film which acts as an insulating layer, and does not necessarily mean that the CIS films are not photo-active. In theory, determining the photovoltage from the CIS film would determine whether or not the CIS is photo-active but this is exceedingly difficult. The measurement is not straightforward, and may not be possible using the three-electrode electrochemical cell, a limitation of the technique, hence it was not undertaken in this study.

### **3.1.3 Discussion of the differences between films deposited on aluminium and glass substrates**

The difference in thickness of the films deposited on the aluminium and FTO substrates can be explained by the difference in conductivity of the two materials. The Al has higher conductivity than the FTO which could result in different electrostatic fields. This in turn could affect the spray cone. The Al could have a larger cone angle as the columbic repulsion between the droplets is stronger and results in a longer cascade of particle splitting than seen in the lower intensity FTO case where the final particle size is larger. This has been confirmed by

analysis of the images seen in Figure 9 which are from the laser particle visualisation study.

The pictures in Figure 9 show the difference in the cone shape when spraying onto aluminium (Figure 9A) and FTO (Figure 9B). Figure 9A shows a larger cone area while the Figure 9B shows a more compact aerosol cone. This is consistent with the film thickness results obtained using XRD, SEM and RBS which show the aluminium substrate to have a thinner CIS layer than that seen on the FTO substrate. The more dispersed cone area results in the solution being deposited over a larger area but with lower thickness than the more compact cone which concentrates the deposition in a smaller area but with a greater thickness.

### **3.2 Glass and Steel Needles**

To study the effect of needle type on the film properties, the spray conditions were fixed; needle-substrate distance = 50 mm, deposition temperature 450 °C, applied voltage = 18 kV and flow rate = 100 µl/min. The XRD patterns of the films deposited using the two different needles (stainless steel and glass) can be seen in Figure 10. The diffraction pattern was identified as the CIS chalcopyrite structure. No extraneous peaks were observed in the XRD patterns suggesting an absence of other phases. In contrast, impurity phases are observed in samples deposited with other methods such as spray ion layer gas reaction [20] and electrochemical [25].



The SEM pictures of the morphology of two samples deposited with two different needles are shown in Figure 11. On the top, the stainless steel needle produces a film with a rougher layer compared to the film obtained with a glass needle. This suggests a different particle size distribution inside the two aerosol cones probably caused by a different atomisation process of the precursor solutions. The electric field profile is dependant on many factors, one of the most important being the shape of the conductive parts of the needle. For the stainless steel needle this includes both the needle and the electrically conducting precursor solution, whereas for the glass needle only the precursor solution conducts. The high electrical conductivity of the stainless steel needle may dominate the electric field profile and effectively fix the geometry of the spray, making it less sensitive to changes in the shape of the precursor meniscus.

Whereas for the glass needle only the precursor solution conducts and the electric field in the vicinity of the tip is solely defined by the shape of the meniscus. As the high electric field will distort the meniscus during deposition the spray from the glass needle is expected to be more diffuse due to rapid changes in meniscus shape. Figure 12 shows the MiniSIMS depth profiles of 2 films sprayed using a steel and glass needle. The figure shows the profiles of the films desired constituents (Cu, In and S) and the main contaminants (Cr and Fe). For both films the level of the three absorber layer constituents are uniform and of identical concentration (indicated by the same level of intensity in the same matrix system). A difference is seen in the impurity concentration in the CIS films. Cr and Fe, detected at a background level in samples deposited using the glass

needle, are present at higher levels in the films sprayed using the stainless steel needle. It also seems that the contamination increases with the time of deposition as both traces increase towards the surface of the film. This is consistent with the prolonged erosion of the stainless steel needle resulting in greater concentrations of the contaminant elements being introduced into the spray solution.

The acidity of the spray solution results in the degradation of the integrity of the internal walls of the steel needle as shown by the optical microscopy images of the cross section of a used steel needle in Figure 13. The solution must result in de-passivation of the inside of the stainless steel needle. This could occur when the protective chromium oxide layer has been attacked by the solution, to then give subsurface corrosion.

Figure 14 shows two typical photo-voltammogram responses for thin films under pulsed white light illumination where the light is on for a shorter period than it is off. The thin film deposited with the glass needle shows a negative photocurrent increasing with applied negative voltage. At greater negative potentials the Fermi level in the film is higher, filling trap states and increasing the band bending at the film electrolyte interface thus giving an increased photocurrent. Also, the photocurrent rise time is fast, which indicates good quality material. The dark current is small except at negative voltages above -0.5 V where the dark current increases. This is attributed to different causes such as reduction and dissolution of the material (which dissolves into the electrolyte), pinholes or cracks going through to the substrate so the redox couple reacts directly with the substrate, and finally that the material is highly doped thus electrons can tunnel through the

barrier. The thin film deposited with the stainless steel needle has a larger dark current and has only a small photo-response, indicating that the material is of poor quality.

## 4 Conclusions

The results of the study on the needle and substrate materials are definitive. Neither the samples deposited with a stainless steel needle nor the samples sprayed on metal substrates show any photoconductivity. This behaviour is attributed to two different causes: the stainless steel needle contaminating the solution and thus the as-deposited films; secondly the metal substrate is corroded by the acid solution resulting in an insulating barrier between the film and the substrate. In this case the films could be photoactive but the current could be blocked by the insulating oxide layer and thus can't be measured. The photovoltage could be measured instead of the current. Unfortunately these measurements are very difficult in a three-electrode electrochemical cell.

## 5 Acknowledgement

This work was funded by EPSRC under grant GR/S74171/01

## 6 References

1. A.N. Tiwari, D.K. Pandya and K.L. Chopra, Sol. Cells 22 (1987) 263.
2. L.Y. Sun, L.L. Kazmerski, A.H. Clark, P.J. Ireland and D.W. Morton, J. Vac. Sci. Technol. 15 (1978) 265.
3. G.-C. Park, H.-D. Chung, C.-D. Kim, H.-R. Park, W.-J. Jeong, J.-U. Kim, H.-B. Gu and K.-S. Lee, Sol. Energy Mater. Sol. Cells 49 (1997) 365

4. T. Yukawa, K. Kuwabara and K. Koumoto, *Thin Solid Films* 286 (1996) 151.
5. Y. Yahua, L. Yingchun, F. Ling, Z. Haihua, L. Deren, L. Zhichao and Z. Shaoxiong Proceedings of ISES Solar World Congress 2007: Solar Energy and Human Settlement, Beijing, China, 18-21 September 2007, 1082-1084
6. M.A. Contreras, K.R. AbuShama, F. Hasoon, D.L. Young, B. Egaas and R. Noufi, *Prog Photovoltaics* 13 (2005) 209.
7. W. Zhendong, M. Xiaoliang, L. Juan, S. Dalin and C. Guorong J. *Alloys Compd.* 487 (2009) L1.
8. Y.B. He, A. Polity, H.R. Alves, I. Österreicher, W. Kriegseis, D. Pfisterer, B.K. Meyer and M. Hardt, *Thin Solid Films* 403-404 (2002) 62
9. Y. Akaki, H. Komaki, K. Yoshino and T. Ikari, *J. Vac. Sci. Technol. A.* 20 (2002) 1486.
10. I. Shigeru, K. Ryo, Y. Tetsuro and M. Michio, *J. Electrochem. Soc.* 157 (2010) B99.
11. P.J. Dale, A.P. Samantilleke, G. Zoppi, I. Forbes, S. Roncallo and L.M. Peter, *ECS Trans.* 6 (2007) 535
12. M. Sahal, B. Marí and M. Mollar, *Thin Solid Films* 517 (2009) 2202.
13. S. Roncallo, J.D. Painter, M.A. Cousin, K.D. Rogers and D.W. Lane, 21<sup>st</sup> EU-PVSEC, Dresden, Germany, 4 - 8 September 2006, 1973.
14. S. Roncallo, J.D. Painter, M.A. Cousins, D.W. Lane and K.D. Rogers, *Thin Solid Films* 516 (2008) 8493
15. S. Roncallo, J.D. Painter, S.A. Ritchie, M.A. Cousins, M.V. Finnis and K.D. Rogers, *Thin Solid Films* 518 (2010) 4821.
16. A. Andersson, N. Johansson, P. Broms, N. Yu, D. Lupo and W.R. Salaneck, *Adv. Mater.* 10 (1998) 859.
17. K. Choy, W. Bai, S. Clarojrochkul and B.C.H. Steele, *J. Power Sources* 71 1-2 (1998) 361.
18. R. Neagu, D. Perednis, A. Princivalle and E. Djurado, *Solid State Ion.* 177 (2006) 1981.

19. R. Neagu, D. Perednis, A. Princivalle and E. Djurado, *Surf. Coat. Technol.* 200 (2006) 6815.
20. C. Camus, N.A. Allsop, S.E. Gledhill, W. Böhne, J. Rohrich, I. Lauermann, M.C. Lux-Steiner and C.H. Fischer, *Thin Solid Films* 516 (2008) 7026.
21. M. Krunk, O. Kijatkina, A. Mere, T. Varema, I. Oja and V. Mikli, *Sol. Energy Mater. Sol. Cells* 87 (2005) 207.
22. T. Wilhelm, B. Berenguier, M. Aggour, M. Kanis and H.J. Lewerenz, *C. R. Chim.* 9 (2006) 294.
23. J.J. Scragg, P.J. Dale and L.M. Peter, *Thin Solid Films* 517 (2009) 2481.
24. M. Mayer, *SIMNRA User's Guide*, Report IPP 9/113 (1997), Max-Planck-Institut für Plasmaphysik, Garching, Germany.
25. B. Asenjo, A.M. Chaparro, M.T. Gutiérrez and J. Herrero, *Thin Solid Films* 511-512 (2006) 117.

#### List of Figures

Figure 1: Schematic of the setup used for particle image velocimetry (PIV) analysis of the spray cone

Figure 2: X-ray diffraction pattern of the sample G3 deposited on FTO at 18 kV, 450 ° C and 25  $\mu\text{l}/\text{min}$ . The planes have been assigned using the CIS chalcopyrite structure

Figure 3: Cross section of the sample deposited using an applied voltage of 18 kV, solution flow rate of 25  $\mu\text{l}/\text{min}$  and deposition time of 12 hours

Figure 4: SEM pictures of the sample deposited at 14 kV (applied voltage) and 100  $\mu\text{l}/\text{min}$  (solution flow rate) for 3 hours (deposition time)

Figure 5: EQE curve of the sample G3 and plot used to determine the band gap energy (top right corner).

Figure 6: Diffractogram of the  $\text{CuInS}_2$  deposited at 18 kV, 450 °C and 25  $\mu\text{l}/\text{min}$  on aluminium substrates

Figure 7: Close up of Figure 6 shows the additional un-identified peaks (+) observed on the samples deposited on aluminium substrates.

Figure 8: RBS spectra of the sample Al3 deposited at 18 kV applied voltage and 25  $\mu\text{l}/\text{min}$  solution flow rate for 3 hours

Figure 9: PIV images of the aerosol cone generated when spraying onto FTO (A) and aluminium (B) substrates

Figure 10: Diffractogram of the  $\text{CuInS}_2$  as-deposited films sprayed using glass and stainless steel needles. The samples were deposited using a needle-substrate distance = 50 mm, a deposition temperature 450 °C, an applied voltage = 18 kV and flow rate = 100  $\mu\text{l}/\text{min}$

Figure 11: SEM pictures of the  $\text{CuInS}_2$  films deposited using stainless steel needle (top) and glass needle (bottom). The samples were deposited using a needle-substrate distance = 50 mm, a deposition temperature 450  $\mu\text{C}$ , an applied voltage = 18 kV and flow rate = 100  $\mu\text{l}/\text{min}$

Figure 12: Depth profiles of 2 films sprayed on FTO/glass using a stainless steel needle (top) and glass needle (bottom). The samples were deposited using a needle-substrate distance = 50 mm, a deposition temperature 450 °C, an applied voltage = 18 kV and flow rate = 100  $\mu\text{l}/\text{min}$

Figure 13: Cross section images of a stainless steel needle after spray deposition. The images were captured after a deposition period of three hours using a needle-substrate distance = 50 mm, a deposition temperature 450 °C, an

applied voltage = 18 kV, a solution flow rate = 100  $\mu\text{l}/\text{min}$ , solution concentration = 0.21 M and a pH = 2.2

Figure 14: Photo-voltammograms of CIS deposited by glass needle (—) and steel needle (----). The samples were deposited using a needle-substrate distance = 50 mm, a deposition temperature 450  $^{\circ}\text{C}$ , an applied voltage = 18 kV and flow rate = 100  $\mu\text{l}/\text{min}$

List of tables

Table 1: Table of the deposition conditions for the samples sprayed on FTO's

Table 2: Table of the deposition conditions for the samples sprayed on Al substrate

Table 3: Table of the compositional analysis of the samples sprayed on Al (from RBS)

Table 1: Table of the deposition conditions for the samples sprayed on FTO's

Sample	Applied voltage [kV]	Flow rate [ $\mu\text{l}/\text{min}$ ]	Time [h]
G1	18	100	3
G2	18	50	6
G3	18	25	12
G4	16	100	3
G5	16	50	6
G6	16	25	12
G7	14	100	3

G8	14	50	6
G9	14	25	12

Table 2: Table of the deposition conditions for the samples sprayed on Al substrate

Sample	Applied voltage [kV]	Flow rate [ $\mu$ l/min]	Time [h]
A1	18	100	3
A2	18	50	6
A3	18	25	12
A4	16	100	3
A5	16	50	6
A6	16	25	12
A7	14	100	3
A8	14	50	6
A9	14	25	12

Table 3: Table of the compositional analysis of the samples sprayed on Al (from RBS)

Sample	Cu [atomic fraction]	error	In [atomic fraction]	error	S [atomic fraction]	error	Film Thickness [ $\mu$ m]	error
A1	0.24	0.02	0.16	0.01	0.60	0.02	0.48	0.02
A2	0.22	0.01	0.25	0.02	0.49	0.1	0.53	0.01
A3	0.21	0.01	0.23	0.02	0.58	0.02	0.50	0.01
A4	0.26	0.02	0.25	0.02	0.49	0.01	0.53	0.02
A5	0.24	0.01	0.16	0.01	0.60	0.01	0.41	0.03
A6	0.28	0.02	0.22	0.01	0.50	0.02	0.62	0.01
A7	0.28	0.02	0.22	0.02	0.50	0.02	0.89	0.01
A8	0.22	0.01	0.25	0.01	0.53	0.03	0.89	0.03
A9	0.28	0.01	0.22	0.01	0.50	0.03	0.57	0.01



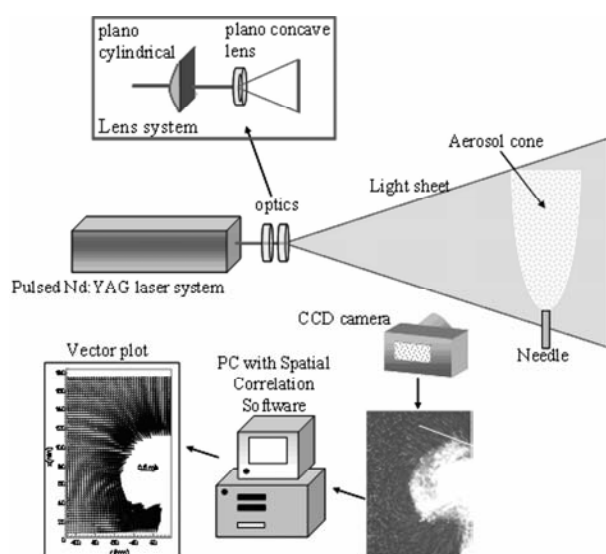


Fig. 1

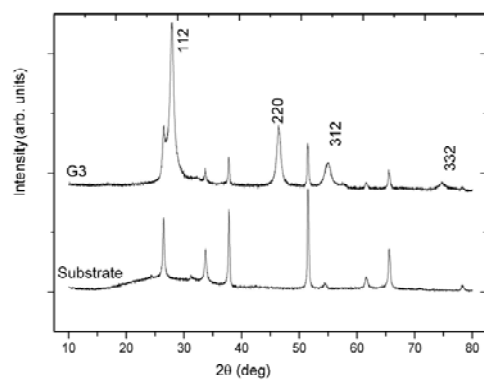


Fig. 2

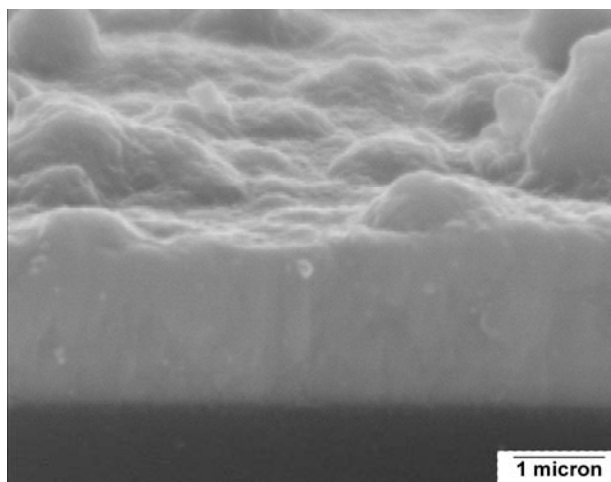


Fig. 3

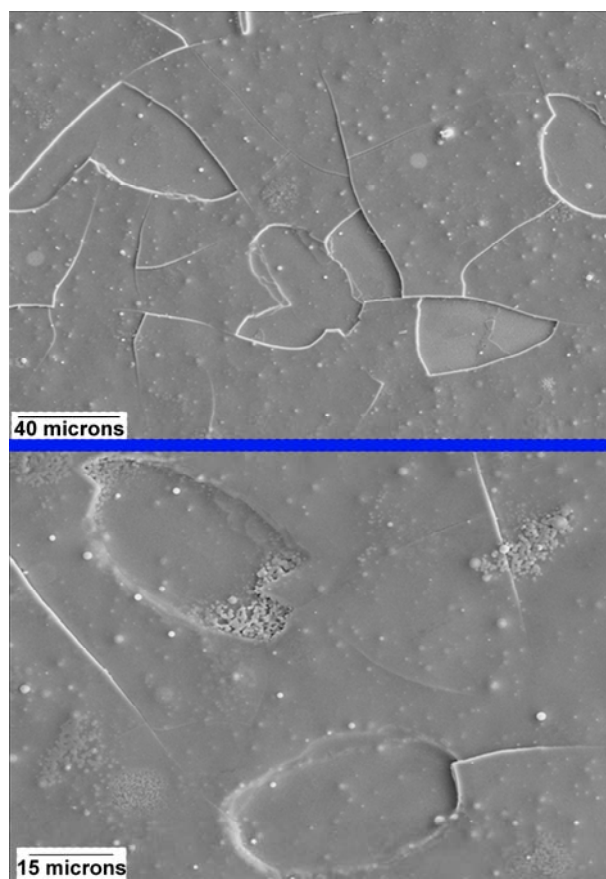


Fig. 4

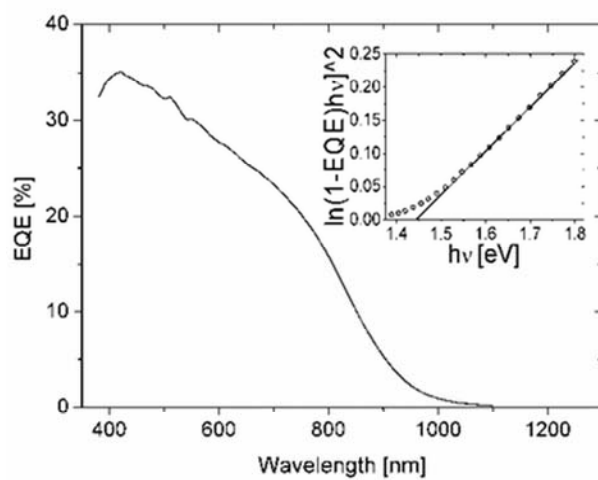


Fig. 5

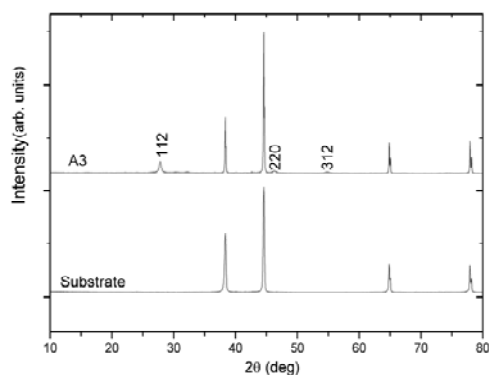


Fig. 6

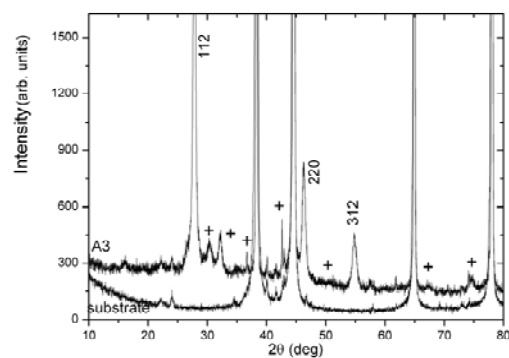


Fig. 7

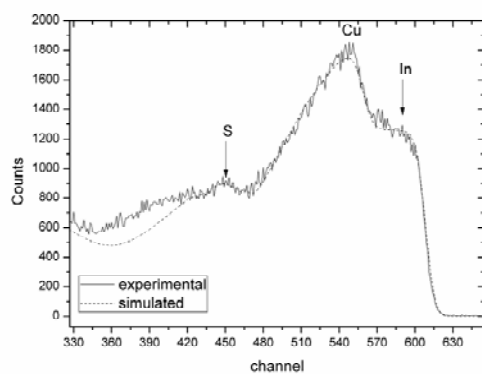


Fig. 8



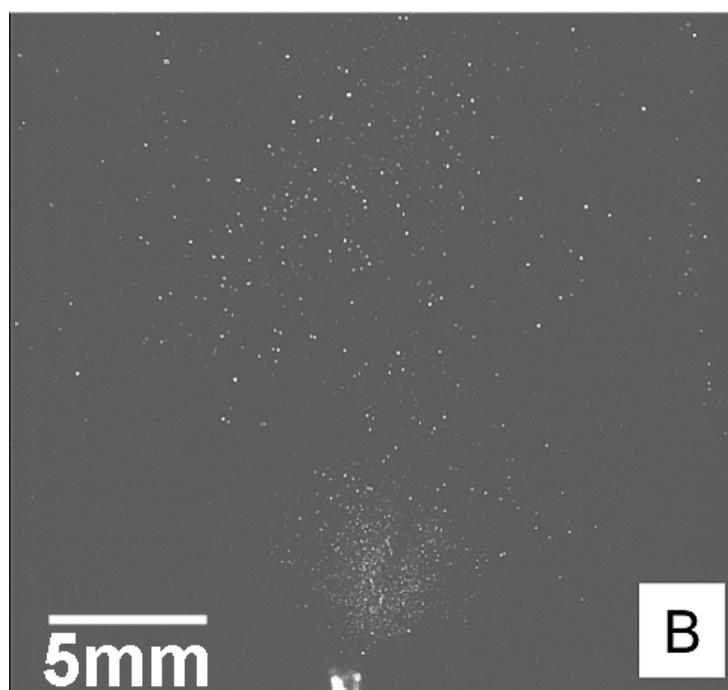
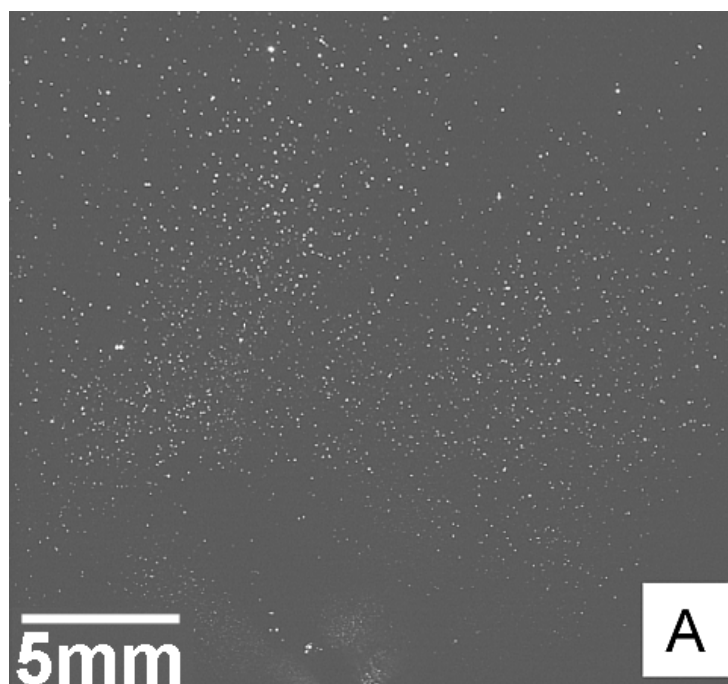


Fig. 9

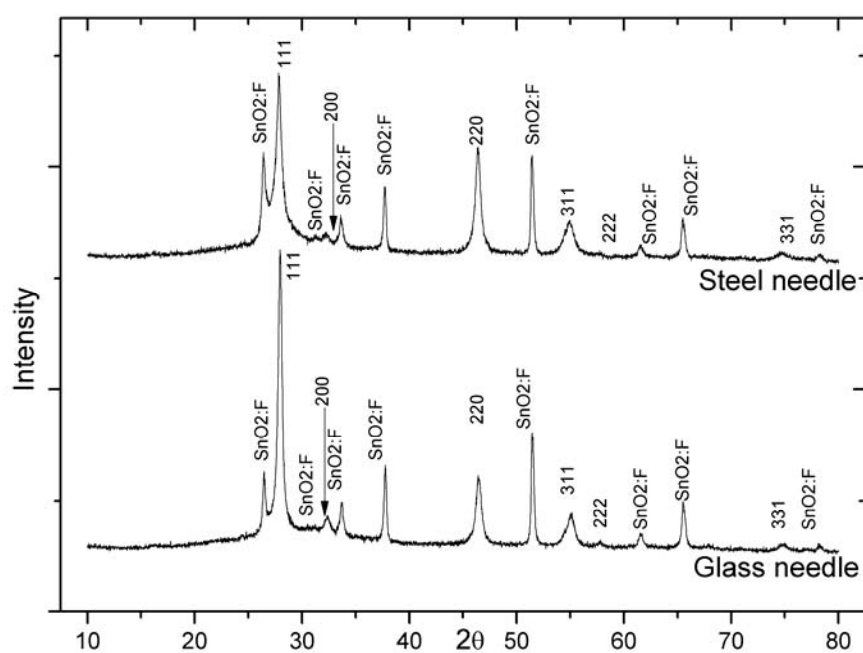


Fig. 10

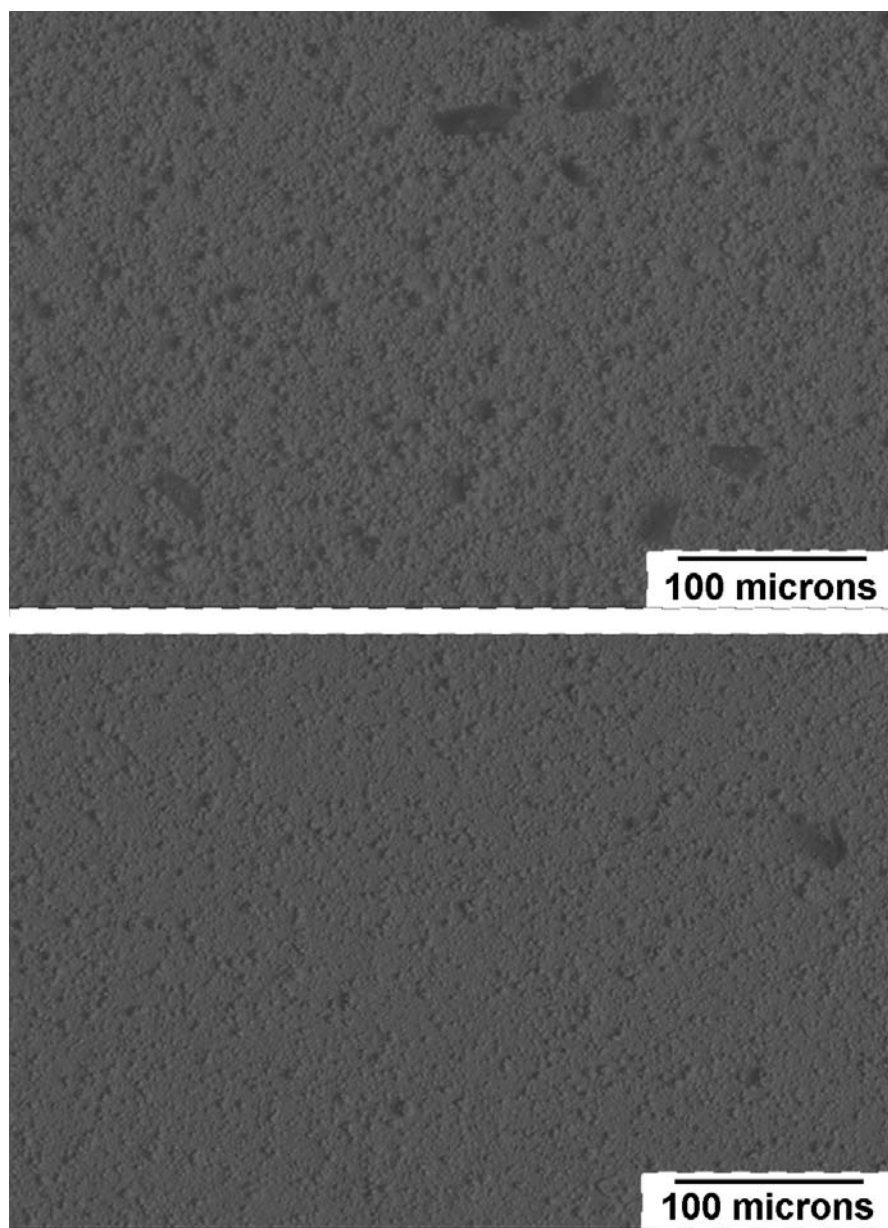


Fig. 11

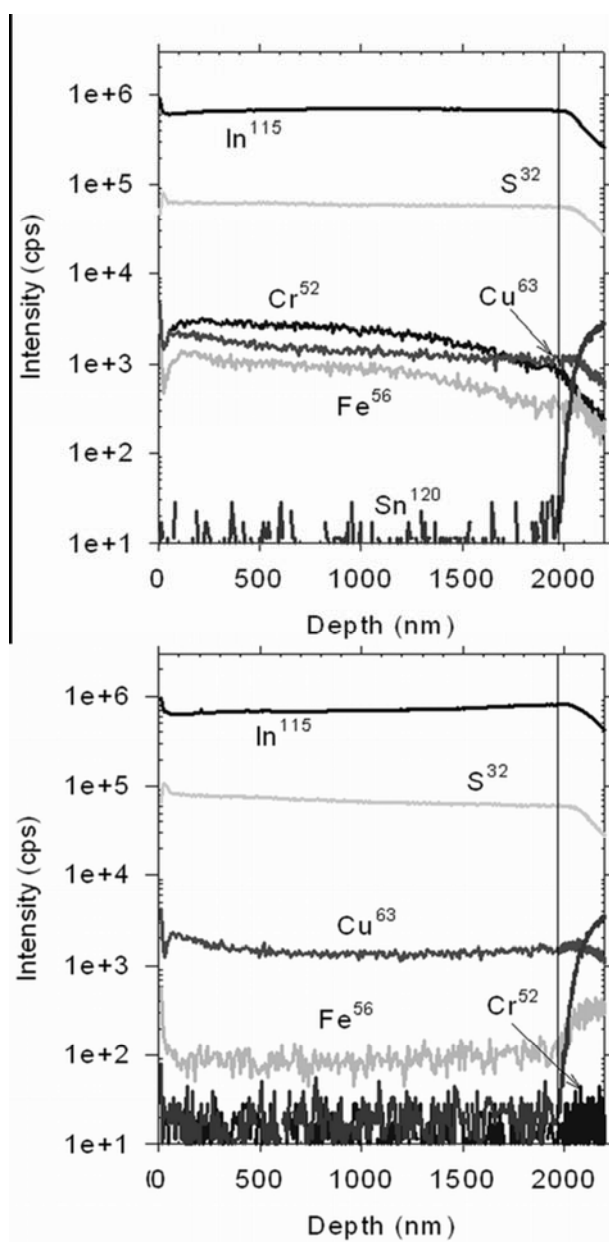


Fig. 12

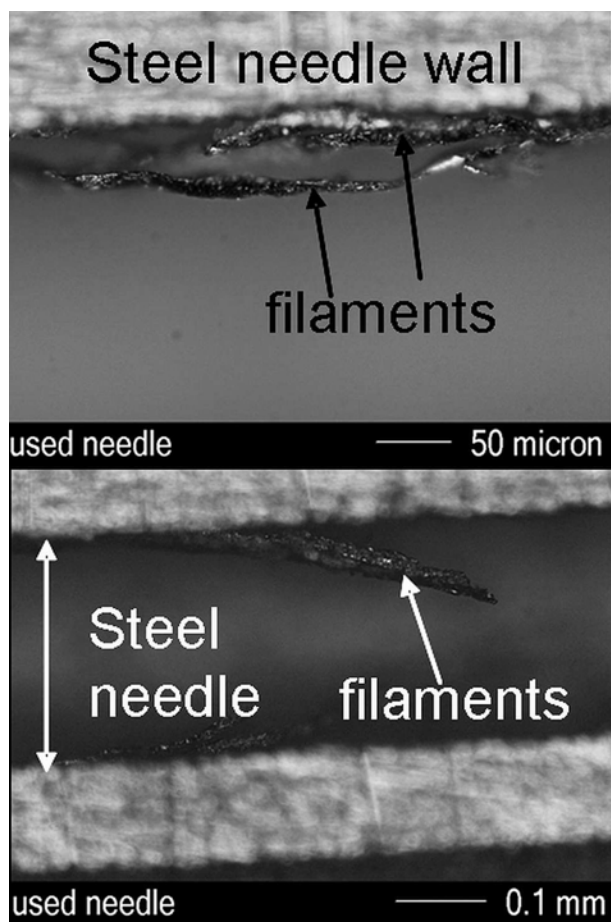


Fig. 13

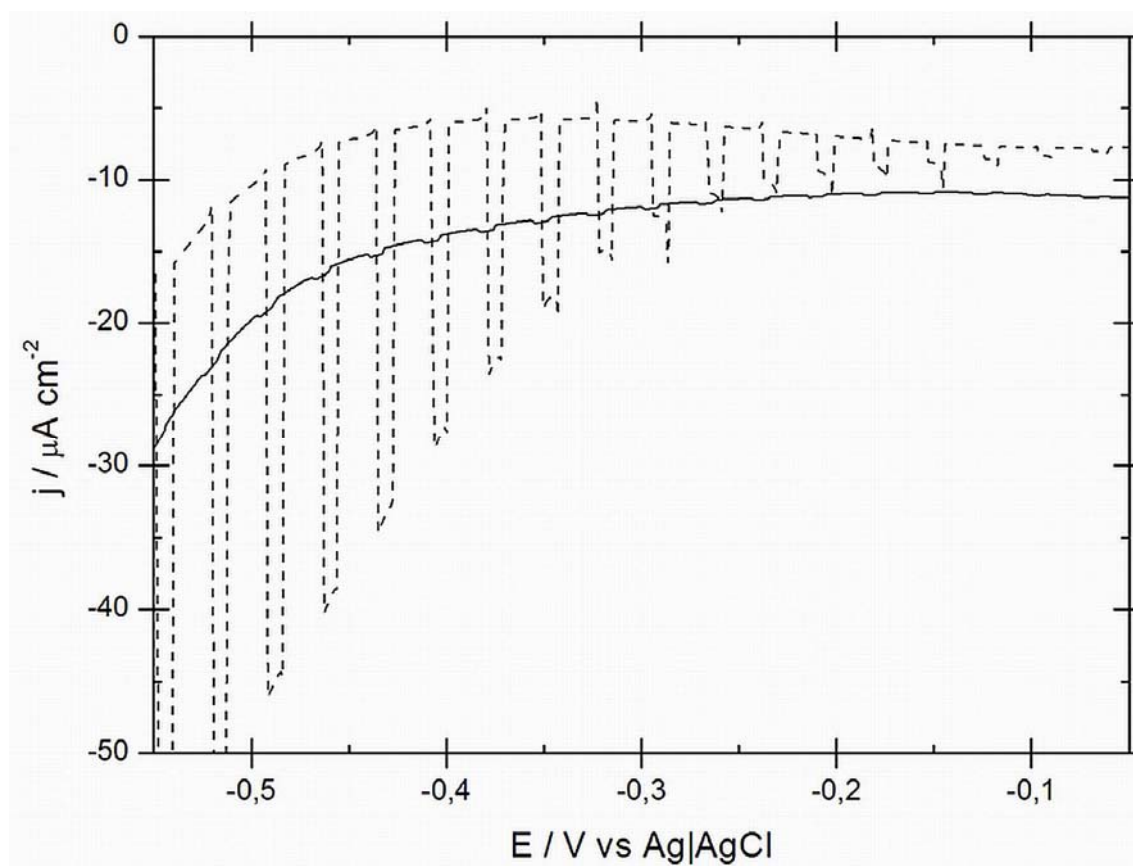


Fig. 14